A Three-dimensional Finite Element Model for Arterial Clamping

Thomas C. Gasser

Christian A. J. Schulze-Bauer

Gerhard A. Holzapfel[1]

Graz University of Technology
Institute for Structural
Analysis–Computational Biomechanics
Schiesstattgasse 14-B, A-8010 Graz, Austria
URL: http://www.cis.tu-graz.ac.at/biomech

Clamp induced injuries of the arterial wall may determine the outcome of surgical procedures. Thus, it is important to investigate the underlying mechanical effects. We present a three-dimensional finite element model, which allows the study of the mechanical response of an artery–treated as a two-layer tube-during arterial clamping. The important residual stresses, which are associated with the load-free configuration of the artery, are also considered. In particular, the finite element analysis of the deformation process of a clamped artery and the associated stress distribution is presented. Within the clamping area a zone of axial tensile peak-stresses was identified, which (may) cause intimal and medial injury. This is an additional injury mechanism, which clearly differs from the commonly assumed wall damage occurring due to compression between the jaws of the clamp. The proposed numerical model provides essential insights into the mechanics of the clamping procedure and the associated injury mechanisms. It allows detailed parameter studies on a virtual clamped artery, which can not be performed with other methodologies. This approach has the potential to identify the most appropriate clamps for certain types of arteries and to guide optimal clamp design. [DOI: 10.1115/1.1485284]

Keywords: Arterial Clamp, Arterial Wall Mechanics, Arterial Histology, Structural Model, Residual Stress, Finite Element Analysis, Finite Element Model

1 Motivation and Introduction

Arterial clamps are chosen to compress arteries during surgery so that blood flow is arrested. Arterial compression, however, may lead to injuries of the vessel wall, which are associated with a variety of severe short-term and long-term complications. For example, clamp induced injuries may cause spontaneous occlusion of the vessel after the operation, which leads to infarction of the downstream tissues. Therefore, surgeons require arterial clamps that allow efficient compression and cause only minimal injury. Severity and distribution of injuries depend on (i) the arterial type [1,2], the geometry and the nonlinear and anisotropic material behavior of the clamped multi-layered artery, (ii) the design of the chosen clamp [3–7] and (iii) the applied clamping forces [2,6,8,9]. The optimization of this mechanical problem requires a numerical model, which considers appropriately all decisive factors. Yet, such a model is not available in the literature to date.

Appropriate numerical models may lead to substantial improvements of arterial clamp designs, and thus are of potential interest for surgeons and clamp suppliers. In the past the demand for appropriate arterial clamps has led to a great variety of different designs and techniques. A suitable clamp design provides easy handling, good vessel grip and efficient vessel occlusion, and it is aimed to minimize arterial injuries. Clamps are named after their inventors as, for example, *Blalock, Cooley, DeBakey, Fogarty, Potts, Satinsky*, etc. They are available in different sizes with straight, curved or angled branches. Their jaws may be plain or have spikes, and they may be silicone filled.

The existing designs are based on surgical intuition rather than on mechanical considerations. Consequently, the effects of clamping and the suitability of clamp designs have been investigated by means of experimental studies rather than by mechanical analyses. To the authors' knowledge, only [10] presented a mathematical approach with the goal to determine the minimum vascular occlusive force. However, this simplifying analytical model does not consider the crucial constitutive behavior of arterial walls. Thus, it is incapable of calculating wall stresses. Despite the clinical significance of arterial clamping there are relatively few studies, which are concerned with its local effects. Most of the experimental investigations are animal studies and focus on morphological changes. The observed injuries range from mild damage, which involves only the intima, to severe damage with total disruptions of the media, layer delaminations and even total wall disruptions with associated bleeding. In addition, long-term changes such as stenoses [11] and intimal hyperplasia–excessive thickening of the intima due to tissue growth [1]-have been observed. Beside structural changes also functional changes of clamped arteries have been investigated, for example, the ability to relax or contract upon application of certain drugs [7,8] and the ability to inhibit blood clotting [12,13]. The influences of the clamping force [2,6,8,9] and of the duration of clamping [14] have been studied. Moreover, comparisons of different types of arteries [2] and different clamp designs [3–7] in regard to clamp induced wall injury have been performed.

These studies have identified the types and the consequences of clamp induced injuries and thus have demonstrated the importance of proper clamp designs. However, experimental studies are afflicted with a number of disadvantages. They are expensive and time-consuming and it is disputable if results of animal arteries are representative for human arteries. The significance of experimental studies is definitely restricted to the chosen arteries, instruments and clamping conditions. A fundamental shortcoming is that the results of existing experimental studies do not provide insights into the mechanical process of arterial clamping. The latter is determined by the three-dimensional stress-strain distributions in the clamped arterial wall.

To overcome these shortcomings we developed a three-dimensional finite element model for arterial clamping. The essential approach is to model the artery as a two-layer fiber-reinforced material with the fibers corresponding to the collagenous component of the material. The two layers represent the media (the middle layer of the artery) and the adventitia (the outer layer). The

[1]Corresponding author: e-mail: gh@biomech.tu-graz.ac.at
Contributed by the Bioengineering Division for publication in the JOURNAL OF BIOMECHANICAL ENGINEERING. Manuscript received April 5, 2001; revised manuscript received March 1, 2002. Associate Editor: J. D. Humphrey.

model captures nonlinear elastic and anisotropic material behavior within the large strain domain. The very important residual stresses in an artery *in vitro* are also accounted for. The numerical model provides a tool for studying the layer-specific mechanical response of clamped arteries subject to an arbitrarily chosen clamp design. We present the three-dimensional deformation and stress distributions in the arterial wall during the clamping procedure. The observed effects and their clinical implications are discussed. Finally, limitations of the proposed model are specified.

2 Methods

2.1 Arterial Histology. Arteries are thick-walled cylindrical tubes, which consist of three concentric layers: the innermost *intima*, the *media* and the outermost *adventitia*. Basically, all layers have a common general composition. They consist of *cells* and their surrounding, which is called *extracellular matrix*. The latter is subdivided in a fibrous matrix (collagen and elastin fibers) and a non-fibrous matrix.

Elastin ''units'' assemble to irregular meshes, which seem to behave as *isotropic* materials. Collagen ''units'' arrange as highly ordered fibers, which yield to anisotropic mechanical responses. Among the intracellular structural proteins only the contractile actomyosine system of the smooth muscle cells in the media creates highly ordered fibrillar structures that account for macroscopic anisotropy.

Intimal, medial and adventitial tissues have distinct physiological tasks. These tissues differ from the types of their histological constituents (cells and extracellular matrix), the respective amount and their spatial orientation. Their fibrous constituents are arranged in counter-rotating helices with layer-specific pitches. Thus, the constitutive behavior of all layers may be described as a fiber-matrix model, which consists of an isotropic ground substance and therein-embedded families of fibers, which account for the anisotropic response. The consideration of the layer-specific preferred directions of oriented histological (major) constituents leads to a histostructural constitutive model.

Smooth muscle cells in the media allow active contractions of the vessel, which modify its mechanical behavior. Hence, the mechanical response of arteries may be specified as *active* or *passive* according to the contractile state of the arterial musculature. Data on the active response of arteries are hardly available in the literature. In the presented model we use data of the passive response of human arteries.

The histological characteristics of arteries depend strongly on their topographical position. Roughly, arteries may be subdivided into two types: *elastic* and *muscular*. ''Elastic'' arteries contain large amounts of elastin in the medial layer and have a very thin adventitia. In ''muscular'' arteries smooth muscle cells are the major constituent of the media and the wall thickness-diameter ratio is greater than in ''elastic'' arteries. For more details on the subject of arterial histology the reader is referred to, for example, [15–17].

2.2 A Structural Model for the Arterial Wall. Our constitutive model describes the *passive* mechanical behavior of *healthy* and *young* arterial walls, which is governed mainly by elastin and collagen fibers (see, for example, [18]). In order to predict three-dimensional distributions of stresses and strains of arterial walls we use a structural model recently proposed by [17,19]. For an extension of the structural model to the finite viscoelastic domain, as it is necessary for arterial walls of the *muscular* type, the reader is referred to the work by Holzapfel and Gasser [20]. For mechanical loadings which are far beyond the physiological domain, permanent deformation occurs, and more sophisticated models have to be chosen (for an extension of the present model to the elastoplastic domain, see [21]).

We consider the arterial wall as a two-layer fiber-reinforced structure, the two layers represent the media and the adventitia. The intima is neglected, since in healthy arteries its thickness and mechanical strength are insignificant compared with the medial and adventitial layers (for more details and references see Humphrey [16], pp. 40,41). The media and adventitia are treated as thick-walled circular composite tubes, which are reinforced by two families of collagen fibers symmetrically disposed with respect to the cylinder axis. Hence, the tubes behave *cylindrically orthotropic* within the finite elastic strain domain. This consideration is generally accepted in the literature (see, for example, the early work by Patel and Fry [22] on the elastic symmetry of arterial segments in dogs).

From experimental observations of arteries it is known that they behave nearly incompressible [23] within the physiological range of deformation (the bulk modulus tends to infinity). For this physical reason and for reasons which are clear from the computational point of view, it seems to be most beneficial to choose a *decoupled* representation of the free-energy function Ψ at any reference point $\mathbf{X}$ of the biological soft tissue. The free energy Ψ is defined per unit volume associated with the *reference (stress-free)* configuration. The isothermal elastic deformation (process) from the reference to the current configuration of the media M and the adventitia A is assumed to be characterized by the penalty form

$$\Psi_j = U_j(J) + \overline{\Psi}_j(\overline{\mathbf{C}}, \mathbf{A}_1, \mathbf{A}_2), \quad j = \mathrm{M,A}. \tag{1}$$

The scalar-valued functions U_j are motivated mathematically and $\overline{\Psi}_j$ is responsible for the isochoric elastic response of the material. All these functions (must) satisfy the requirement of objectivity [24].

According to Flory [25] and Ogden [26], the continuum theory is based on the multiplicative decomposition of the deformation gradient $\mathbf{F} = J^{1/3}\overline{\mathbf{F}}$ into a dilatational part $J^{1/3}\mathbf{I}$ and a distortional part $\overline{\mathbf{F}}$, with the second-order unit tensor $\mathbf{I}$ and the local volume ratio $J = \det \mathbf{F} > 0$. The strain measure

$$\overline{\mathbf{C}} = \overline{\mathbf{F}}^{\mathrm{T}}\,\overline{\mathbf{F}} \quad \text{with} \quad \det \overline{\mathbf{C}} = 1, \tag{2}$$

as introduced in Eq. (1), denotes the modified right Cauchy-Green tensor. At any $\mathbf{X}$ the structure of the artery is characterized by the two (second-order) tensors $\mathbf{A}_1$ and $\mathbf{A}_2$. They are defined as the tensor products $\mathbf{a}_{0i} \otimes \mathbf{a}_{0i}$, where $\mathbf{a}_{0i}$, $i = 1, 2$, are two unit vectors ($|\mathbf{a}_{0i}| = 1$) describing the mean orientations of the families of collagen fibers in the reference configuration of the tissue.

We require that U_j are *strictly convex* functions of the form

$$U_j = \frac{\kappa_j}{2}(J-1)^2, \quad j = \mathrm{M,A}, \tag{3}$$

taking on its unique minimum at $J = 1$. The parameters $\kappa_j > 0$ may be viewed as bulk moduli. Since we regard the artery as an incompressible material within the physiological range of deformation, κ serves as a user-specified *penalty* parameter which has no physical relevance (for $\kappa \to \infty$, expression (1) may be viewed as the potential for the incompressible limit, with $J = 1$).

We now focus attention on the description of the isochoric deformation behavior and express the strain-energy functions $\overline{\Psi}_j$ through a set of independent invariants. We use the *same* form of the function (but a different set of material parameters) to model adventitial and medial responses, which have similar mechanical characteristics [27]. Thus, we suggest the simple additive split

$$\overline{\Psi}_j = \frac{c_j}{2}(\overline{I}_1 - 3) + \frac{k_{1j}}{2k_{2j}}\{\exp[k_{2j}(\overline{I}_{1j}^{\star} - 1)^2] - 1\} + \frac{k_{1j}}{2k_{2j}}\{\exp[k_{2j}(\overline{I}_{2j}^{\star} - 1)^2] - 1\}, \quad j = \mathrm{M,A} \tag{4}$$

of $\overline{\Psi}_j$ into parts associated with *iso*tropic and *aniso*tropic contributions to the strain energy [28]. The specific form of the two-layer model (4) requires a set of three (positive) material param-

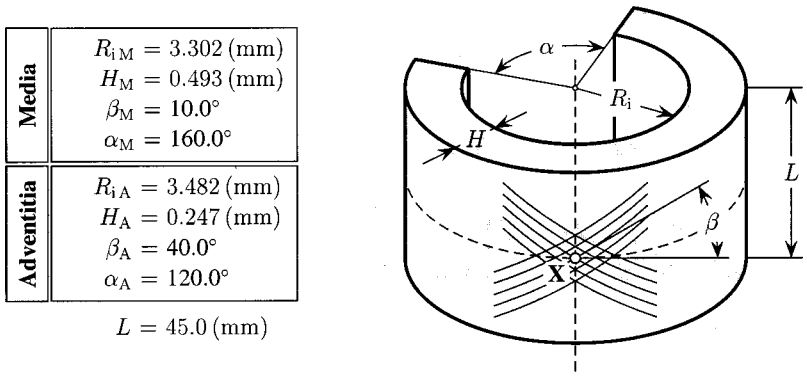

Fig. 1 Opened-up reference (stress-free) configuration of an arterial layer and associated geometrical data for the media and adventitia

eters c_M, k_{1M}, k_{2M} for the media M, and three (positive) material parameters c_A, k_{1A}, k_{2A} for the adventitia A. Note that the material parameters c_i, k_{1i} are stress-like and k_{2j}, $j=$M,A, are dimensionless. The (isotropic) neo-Hookean part of $\overline{\Psi}_j$ we mainly associate with the mechanical response of the *non-collagenous matrix material*, which is the predominant load-bearing material at lower strains (the collagen fibers of arterial walls store little strain energy at lower strains). At higher strains, however, the *collagen fibers* become load-bearing [29] and energy is stored in the fibers. This (anisotropic) mechanical response is described by the exponential terms of function (4). Hence, the material parameters are (roughly) associated with the underlying histological structure.

In (4) we introduced $\overline{I}_1=\overline{\mathbf{C}}:\mathbf{I}$ for the first (principal) invariant of $\overline{\mathbf{C}}$ (describing isotropy), and the definitions

$$\overline{I}^{\star}_{1,j}(\overline{\mathbf{C}},\mathbf{a}_{01j})=\overline{\mathbf{C}}:\mathbf{A}_{1j} \quad \overline{I}^{\star}_{2j}(\overline{\mathbf{C}},\mathbf{a}_{02j})=\overline{\mathbf{C}}:\mathbf{A}_{2j}\,, \quad j=\text{M,A} \tag{5}$$

of the invariants associated with the anisotropic deformation response of the media and adventitia. The invariants $\overline{I}^{\star}_1$ and $\overline{I}^{\star}_2$ determine precisely the squares of the stretches in the (fiber) directions of $\mathbf{a}_{01}$ and $\mathbf{a}_{02}$, respectively (for the theoretical background see, for example, [24,30]). We assume that the collagen fibers do not support compressive stresses. Hence, for the case that $\overline{I}^{\star}_1 \leqslant 1$ and $\overline{I}^{\star}_2 \leqslant 1$, the response is similar to that of a rubber-like (purely isotropic) material, described by the neo-Hookean functions $\overline{\Psi}_j = c_j(\overline{I}_1-3)/2$, $j=$M,A.

Finally we employ a cylindrical coordinate system and neglect components of the (collagen fiber) orientation in the radial direction. Then, the components of the (collagen fiber) vectors $\mathbf{a}_{01j}$ and $\mathbf{a}_{02j}$ read in matrix notation

$$[\mathbf{a}_{01j}]=\begin{bmatrix}0\\ \cos\beta_j\\ \sin\beta_j\end{bmatrix}, \quad [\mathbf{a}_{02j}]=\begin{bmatrix}0\\ \cos\beta_j\\ -\sin\beta_j\end{bmatrix}, \quad j=\text{M,A}, \tag{6}$$

and β_j, $j=$M, A, are the angles between the collagen fibers and the circumferential direction in the media and adventitia (see Fig. 1).

2.3 Decoupled Stress Response. For each arterial layer the (hyper)elastic stress response is derived from the additively decomposed Helmholtz free-energy function (1) in a standard way [24]. We arrive at the Cauchy stress tensor, denoted $\boldsymbol{\sigma}$, to be given in the associated *decoupled* form

$$\boldsymbol{\sigma}_j = p_j\mathbf{I}+\overline{\boldsymbol{\sigma}}_j\,, \quad j=\text{M,A} \tag{7}$$

for the respective media M and adventitia A, with the spherical tensors $p_j\mathbf{I}$ and the deviatoric tensors $\overline{\boldsymbol{\sigma}}_j$ of $\boldsymbol{\sigma}_j$ to the Cauchy stresses. In (7) we introduced the expressions

$$p=\frac{\mathrm{d}U(J)}{\mathrm{d}J}, \quad \overline{\boldsymbol{\sigma}}=2J^{-1}\,\mathrm{dev}\left(\overline{\mathbf{F}}\frac{\partial\overline{\Psi}(\overline{\mathbf{C}},\mathbf{A}_1,\mathbf{A}_2)}{\partial\overline{\mathbf{C}}}\overline{\mathbf{F}}^{\mathrm{T}}\right) \tag{8}$$

for the hydrostatic pressure p and the isochoric stress response $\overline{\boldsymbol{\sigma}}$. In Eq. $(8)_2$, $\mathrm{dev}(\bullet)=(\bullet)-1/3[(\bullet):\mathbf{I}]\mathbf{I}$ furnishes the deviatoric operator in the Eulerian description [24]. Considering the particularizations (3) and (4), responsible for the elastic responses of each arterial layer, from (8) we obtain the explicit expressions

$$p=\kappa(J-1), \quad \overline{\boldsymbol{\sigma}}=c\,\mathrm{dev}\,\overline{\mathbf{b}}+\sum_{i=1}^{2}2\,\overline{\psi}_i\,\mathrm{dev}(\mathbf{a}_i\otimes\mathbf{a}_i), \tag{9}$$

where $\overline{\mathbf{b}}=\overline{\mathbf{F}}\overline{\mathbf{F}}^{\mathrm{T}}$ denotes the modified left Cauchy-Green tensor, $\mathbf{a}_i=\overline{\mathbf{F}}\mathbf{a}_{0i}$, $i=1,2$, are the Eulerian counterparts of the unit vectors $\mathbf{a}_{0i}$, and

$$\overline{\psi}_i=\frac{\partial\overline{\Psi}}{\partial\overline{I}^{\star}_i}=k_1(\overline{I}^{\star}_i-1)\{\exp[k_2(\overline{I}^{\star}_i-1)^2]-1\}, \quad i=1,2 \tag{10}$$

denote stress functions.

As seen from expression $(9)_2$ the isochoric stress response consists of purely *isotropic* contributions due to the non-collagenous matrix material (first term), and *anisotropic* contributions due to the two families of fibers, which characterize decoupled stresses (associated only with the fibers).

2.4 Residual Stresses. Arteries, which are excised from the body, are associated with a complex residual stress-state [31]. Experimental investigations show that an arterial ring springs open when cut in a radial direction. Residual stresses (and strains), inherent in many biologic tissues, result from adaptation mechanisms [32,33]. Their considerations have a strong influence on the stress and strain distributions (at physiological condition) across the arterial wall, and on the global pressure/radius response of arteries [17,34–36]. According to the experimental studies by Vossoughi et al. [37] for bovine specimens, the media and adventitia, when separated from the arterial ring and cut in a radial direction, will spring open to opened-up sectors, which, in general, show different opening angles. In this work we assume that these opened-up sectors are the (stress-free and fixed) reference configuration for which the residual stresses are entirely removed.

2.5 Finite Element Analysis. The structural model proposed above has been implemented in Version 7.3 of the multipurpose finite element analysis program FEAP, originally developed by Taylor and documented by [38]. All three-dimensional finite element analyses of arterial clamping have been performed on a HP-J7000 workstation under the UNIX operating system.

2.5.1 Geometry. Since it is essential to incorporate residual stresses (and strains) in the load-free configuration, as motivated above, we use a finite element mesh, which reproduces two independent opened-up reference (stress-free) configurations of the

Table 1 Elastic material parameters c_i, k_{1i}, k_{2i}, i=M,A, for the media M and adventitia A, and penalty parameters κ_i

Media	Adventitia
$c_M = 27.0$(kPa)	$c_A = 2.7$ (kPa)
$k_{1M} = 0.64$(kPa)	$k_{1A} = 5.1$ (kPa)
$k_{2M} = 3.54$ (−)	$k_{2A} = 15.4$ (−)
$\kappa_M = 10^4$ (kPa)	$\kappa_A = 10^4$ (kPa)

media and adventitia. The reference configuration of one arterial layer is taken to correspond to a circular cylindrical tube with opening angle α, wall thickness H, inner radius R_i and length L, as shown in Fig. 1.

We assume that the media occupies 2/3 of the arterial wall thickness and that the collagen fibers are helically wound. Their orientations at a reference point $\mathbf{X}$, characterized by the angle β, are different for each layer. Specific geometrical data for each arterial layer are given in Fig. 1.

The arterial clamp is idealized as a pair of (rigid) cylinders with a radius of 3.0 (mm).

2.5.2 Material Parameters. The set of (elastic) material parameter c_i, k_{1i}, k_{2i}, i=M,A, which are involved in the strain-energy functions (4), were fitted to the experimental data of a human left anterior descending coronary artery (LAD), as given in [39]. For that we have chosen a standard nonlinear *Levenberg-Marquardt* algorithm. Experimental tests indicate that the media is much stiffer than the adventitia [40]. In particular, we set $c_M = 10.0 c_A$ [17]. The (user-specified) penalty parameters κ_i, i=M,A, were chosen to be 10^4 (kPa). The resulting values are summarized in Table 1.

2.5.3 Finite Element Model. For the artery we have chosen a mixed finite element formulation, which is based on a three-field variational principle [41]. It uses *linear* interpolation functions for the displacement field and (the same) *constant* interpolation functions for the independent (dilatation and pressure) variables (which gives the mean dilatation $Q1/P0$-element, a procedure which goes back to Nagtegaal et al. [42]). The volumetric variables are eliminated on the element level. This well-known technique circumvents numerical difficulties (''*locking*'' and ''*checkerboard*'' *phenomena*) which arise from the overstiffening of the system associated with the analysis of *isochoric* constitutive responses of the arterial wall.

Due to the symmetry of the considered geometry and the loading condition of the problem, only a wedge of the artery with 90.0° is discretized by 1200 $Q1/P0$-elements—750 for the media and 450 for the adventitia. Note that the 90.0° wedge is associated with the ''closed'' (unloaded but stressed circular) configuration. The opened-up reference (stress-free) configurations of the media and the adventitia are represented by $(360.0° - \alpha_M)/4 = 50.0°$ and $(360.0° - \alpha_A)/4 = 60.0°$ wedges, respectively. We have chosen eight finite elements across the wall thickness with the same radial dimension within a layer (five for the media and three for the adventitia). We discretized the circumferential and axial directions of one arterial layer by 10 and 15 finite elements, respectively, while we considered a refined mesh around the clamp region. Each node at the media/adventitia interface is linked together. The number of elements used turns out to be sufficient in order to achieve accurate numerical results. The common symmetrical boundary conditions for the structure are applied. During the whole computation the top and bottom faces of the artery are modeled to remain planar.

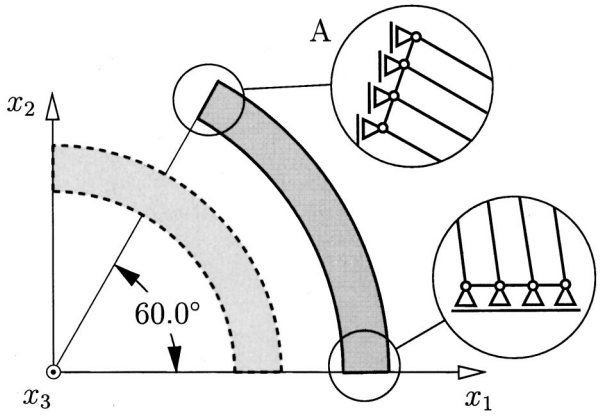

Fig. 2 Boundary conditions in the x_1-x_2 plane for the 60.0° wedge of the stress-free adventitia (solid lines). All nodes of one end of the wedge (close-up view A) are enforced to move in the x_2-direction such that a 90.0° wedge is achieved (dashed lines).

In order to handle the contact problem (the interaction of the boundary of the clamp with the boundary of the artery) we use a *point to surface* strategy. The cylindrical surface of the arterial clamp plays the role of a slave surface modeled by 121 *slave points* which are nodes. The *master surface* is associated with the (outer) boundary of the adventitia, at which contact is expected. It is modeled by master points which are interpolated from 80 four-node (contact) facets.

Finally, frictionless contact is assumed between the arterial boundary and the boundary of the clamp. The control of the penetration between the clamp and the artery is performed by means of the *penalty method*. The discretized (contact) problem is summarized in Table 2.

2.5.4 Loading Process. The whole loading process is separated into three steps:

1. The *stress-free* arterial segments, with geometrical data given in Fig. 1 and (elastic) material parameters and penalty parameters for the media and adventitia as summarized in Table 1, are applied to an initial (pure) bending deformation (for more details see [17]). The boundary conditions in the x_1-x_2 plane are chosen as indicated in Fig. 2, showing an example for the 60.0° wedge of the stress-free adventitia (solid lines). All nodes of one end of the wedge (see the close-up view A in Fig. 2) are enforced to move in the x_2-direction such that a 90.0° wedge is achieved after the bending deformation (dashed lines). This deformation process generates the unloaded but *stressed* circular cylindrical shape of the arterial segment, for which the opening angle $\alpha = 0.0°$. Then, each node at the media/adventitia interface (i.e. the basal lamina externa) is linked together. Finally, we end up with homogeneous stress and strain states in the circumferential and axial directions, which we now use as the

Table 2 Summary of the discretized contact problem (wall/clamp interaction)

Arterial wall (wedge of 90.0°)			Arterial clamp	
$Q1/P0$-elements	Media	750	*Slave* nodes	121
	Adventitia	450		
4-node (contact) facets	Outer boundary of the adventitia (*master* surface)	80		

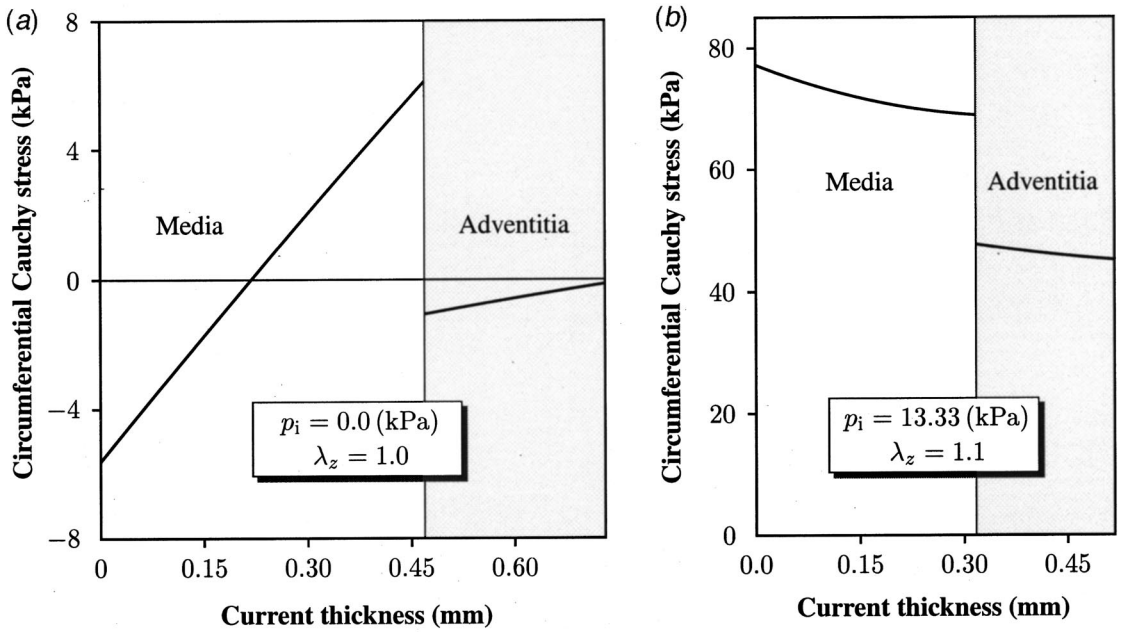

Fig. 3 Distribution of the (circumferential) Cauchy stress through the deformed media and adventitia. (*a*) Residual stresses at the load-free configuration (internal pressure p_i=0.0 (kPa) and axial stretch λ_z=1.0). (*b*) Stresses at the physiological configuration (p_i=13.33 (kPa) and λ_z=1.1). The numerical results are based on the opened-up geometry, as given in Figure 1, and the parameters for the media and adventitia according to Table 1.

reference for subsequent deformation processes.

2. The circular cylindrical two-layer structure is then inflated up to an internal pressure $p_i = 13.33$ (kPa), i.e. 100 mm Hg, which is the mean arterial pressure (averaged over the cardiac cycle) of non-hypertensive subjects at rest [43].

   In general, arteries are stretched significantly in axial direction in their *in situ* configurations (see, for example, the review article [16]). To the authors' knowledge, however, there are no data about axial *in situ* stretches of human coronary arteries available in the literature. For our clamping model we applied an axial stretch of $\lambda_z = 1.1$. This value was measured in preliminary non-published investigations of human coronary arteries (LAD) performed in the authors' laboratory. The stretch is obtained as a displacement-driven process. Thereby, all nodes at $x_3 = 0$ were enforced to have zero displacements in x_3-direction, while all nodes at $x_3 = L$ were enforced to move in x_3-direction according to the given axial stretch of $\lambda_z = 1.1$.

   These loads are considered to be physiological producing the physiological state of deformation.

3. The interaction of the boundary of the clamp with the boundary of the artery is finally computed as a *displacement-driven* problem of the rigid cylinder (clamp). The arterial clamp is placed perpendicular to the axis of the artery (for the geometrical set-up of the clamping process see Figure 4(*a*)).

3 Results

We start by computing the (circumferential) stress distribution through the arterial layers associated with the load-free and physiological configurations. We continue to analyze deformation states of the artery at different displacements of the clamp, and finally, we show the evolution of circumferential and axial stresses at a representative point of the artery during clamping.

3.1 Stress States in the Arterial Layers at the Load-Free and Physiological Configurations. The geometrical data of the arterial segment (Fig. 1) were chosen such that an initial (pure) bending deformation, when applied to the *stress-free* (and fixed) configurations of the layers, generates dimensions of the arterial cross-section of a human LAD, as documented in [39] (unfortunately, therein no geometrical informations of separated opened-up configurations of arterial layers are given). Figure 3(*a*) shows the distribution of the (circumferential) Cauchy stress through the deformed media and adventitia at the load-free (but *stressed*) configuration (α=0.0°). The residual stresses, associated with the load-free configuration, are accumulated during bending. As can be seen from Fig. 3(*a*), the (circumferential) stress distribution in the load-free configuration is mainly determined by the media, which is in agreement with the experimental findings by [44]. This result is intuitive, since the adventitia is very soft in the associated strain domain. Thus, it exhibits only minor bending stiffness and associated residual stresses that are very small. As expected, the inner parts of the media are compressed while its outer parts are extended. In contrast to this finding, the adventitia is compressed throughout its entire thickness. Obviously, this is due to a diameter "mismatch" between media and adventitia.

Figure 3(*b*) shows the circumferential Cauchy stress distribution through the deformed media and adventitia at the physiological configuration at $p_i = 13.33$ (kPa) and $\lambda_z = 1.1$. The radius of the lumen was computed to be 2.52 (mm). In the physiological configuration the stress distributions within the media and the adventitia are relatively smooth, which is an effect of the residual stresses. Again, the media is mechanically predominant, which is necessary for its physiological function. In this state the media can effectively regulate the blood flow due to active contraction.

The curves in Fig. 3 are based on extrapolations of the computed circumferential stress values at the Gauss points to the element nodes, and subsequent averaging of the stress discontinuities at the nodes is performed. In an additional step the averaged nodal stresses are used to get the smooth curves across the wall thickness by means of a polynomial function, as shown in shown in Fig. 3.

3.2 Deformed States of the Clamped Artery. The deformed states of the artery before and after pinching off with a clamp are illustrated in Fig. 4 (the physiological configuration is characterized by state Ⓐ, while deformed state Ⓕ shows

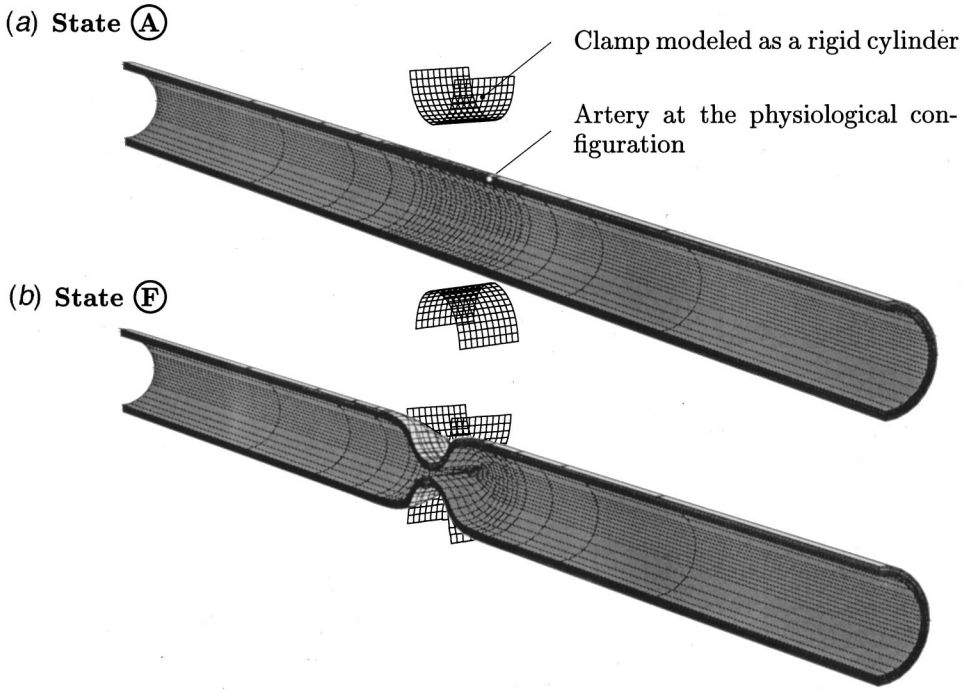

Fig. 4 Deformed states of the artery before and after pinching off with a clamp. (*a*) Artery (media and adventitia) at the physiological configuration with an open clamp. (*b*) Deformed state of the artery, for which the maximum clamp displacement has been applied (full contact between the clamp and the artery).

the nearly occluded artery). In order to clearly demonstrate the deformations the figure takes advantage of the symmetries by showing one half of the artery. As can be seen from Fig. 4(*b*), the region which is affected by the clamping mechanism is relatively small.

Figure 5 illustrates different deformed states of the artery, which occur during the clamping process. State Ⓐ represents again the physiological configuration (before contact with the clamp), while states Ⓑ– Ⓕ show the decrease of the arterial lumen due to clamping.

3.3 Evolution of Stresses in the Artery During Clamping. Three-dimensional finite element analyses showed that in the neighborhood of the clamp, there is a tendency for *circumferential* (Cauchy) stresses in the wall to decrease and for *axial* stresses in the media to increase. To demonstrate the local evolution (change) of stresses in the artery during clamping, we pick a representative point *P*, which is located at the inner surface of the media as indicated in Fig. 6.

In order to show the (local) stress evolutions at *P*, for convenience, we introduce the two (dimensionless) scalar quantities

$$s_\theta = \frac{\sigma_\theta}{\sigma_{\theta\ \mathrm{phys}}}, \quad s_z = \frac{\sigma_z}{\sigma_{z\ \mathrm{phys}}}, \tag{11}$$

which determine the normalized stresses s_θ in the circumferential direction and the normalized stresses s_z in the axial direction. In Eq. (11), σ_θ and σ_z denote the Cauchy stresses in circumferential and axial directions, while $\sigma_{\theta\ \mathrm{phys}}$ and $\sigma_{z\ \mathrm{phys}}$ denote the associated stress quantities at the physiological state Ⓐ, at the same point *P*.

In Fig. 6 the (local) evolutions of the normalized stresses s_θ, s_z with the clamp displacement are plotted. As can be seen the axial stress s_z increases significantly, while the circumferential stress s_θ decreases with progressive clamp displacement. Remarkably, at the final state Ⓕ of the clamping process, with an occlusion of 92.5% referred to the lumen diameter at the physiological state Ⓐ (the maximum dimensions of the lumen are 0.378 (mm) and 5.983 (mm)), the value of the normalized axial stress s_z at the considered point *P* is about four times higher than that at the associated state Ⓐ. Figure 7 illustrates the distribution of

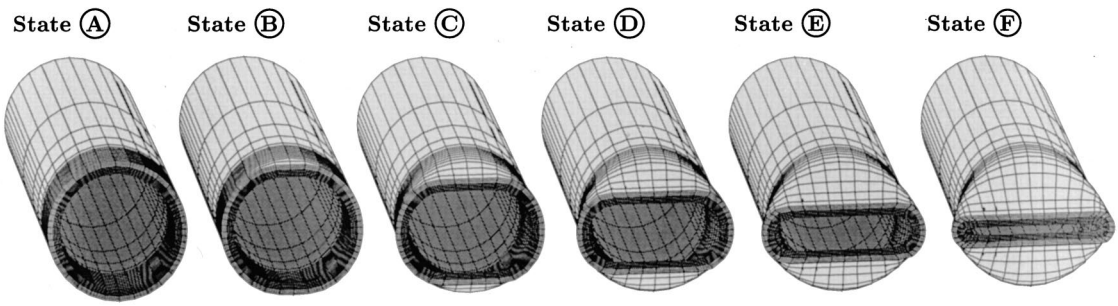

Fig. 5 Deformed states of the artery (media and adventitia) at different displacements of the clamp

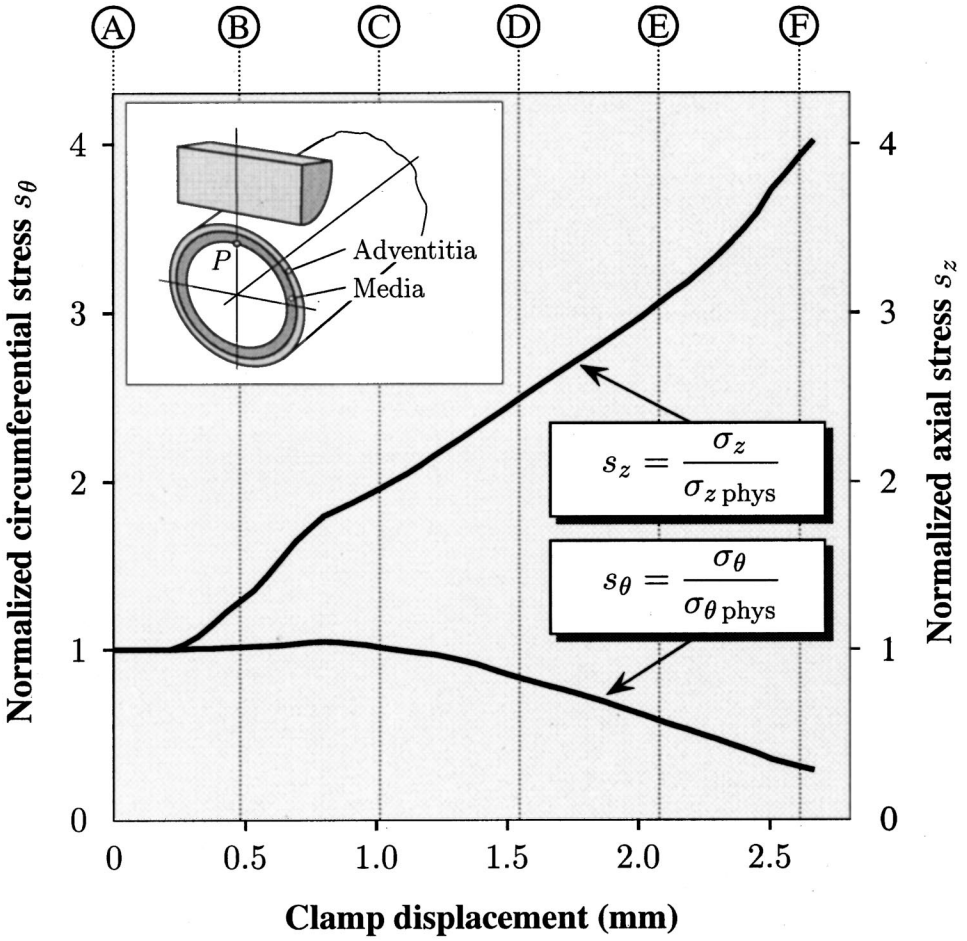

Fig. 6 Evolutions of the normalized circumferential and axial stresses (s_θ,s_z) with the clamp displacement at a certain point *P* located at the inner surface of the media. Note the high increase of s_z with respect to the physiological configuration.

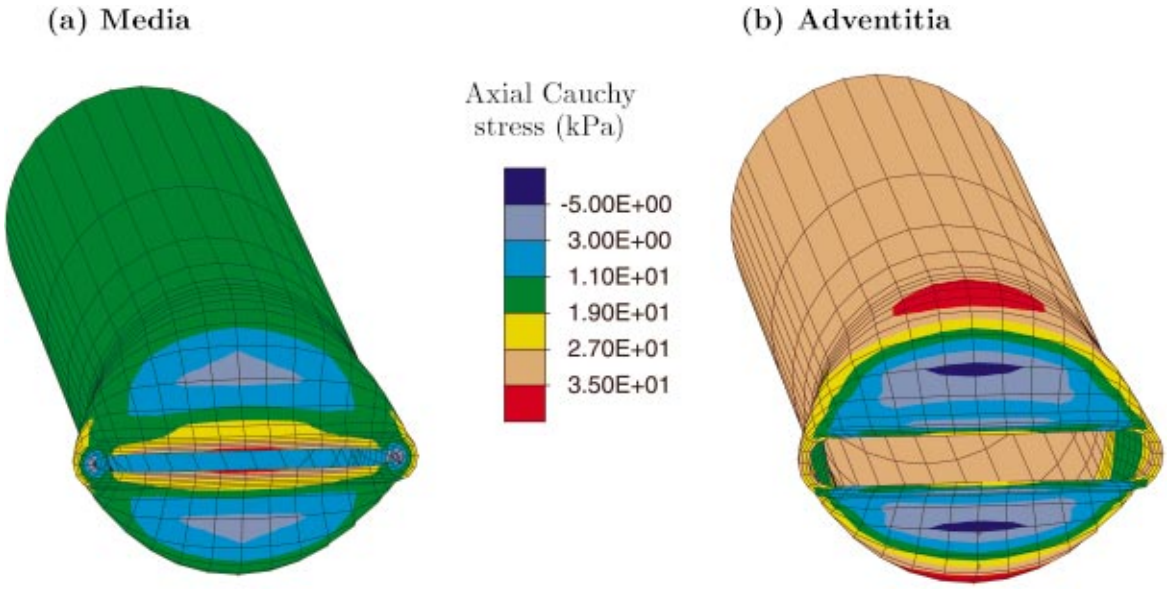

Fig. 7 Distribution of the Axial Cauchy stress in (*a*) the media and (*b*) the adventitia at the final state of the clamping process

the axial Cauchy stress in the media and the adventitia. As can be seen the maximum values of the stresses in the media and adventitia are similar, however their locations are different.

Since the media is not designed to carry high axial loads (it is the task of the adventitia), the clamping process may cause injury in the media. According to the high circumferential stresses at the inner surface of the media one may conclude that the intima is also highly deformed and damaged (compare with the experimental observations [12,45]; see also [3] grading the damage of the arterial wall). It is important to note that the axial stress increase in the media due to clamping is strongly affected by the clamp design.

4 Discussion

4.1 Mechanics of Clamping. Arterial clamping is a mechanical procedure. Thus, its understanding requires an appropriate mechanical model. The key feature of such a model is the arterial wall model. Since arteries are multi-layer structures with layer-specific, anisotropic and nonlinear responses, the arterial wall model must account for these properties. This is an obvious prerequisite in order to yield clinically relevant results. However, to date there are no commercial finite element codes available, which provide results in the large strain domain that cover these typical arterial properties.

To our knowledge the present study is the first to investigate the mechanics of arterial clamping by means of the finite element method. We developed an appropriate three-dimensional finite element model, which is based on a fiber-matrix continuum approach. Currently, we use this model to study the mechanical response of the arterial wall—treated as a two-layer tube. Extension to a three-layer model incorporating pathological intimal changes is a straightforward task. An essential feature of our approach is the consideration of residual stresses, which have a major influence on the distribution of the wall stresses. Material and geometrical parameters of the arterial model, for example, the ratio of the layer thicknesses, the diameter-wall thickness ratio and the axial *in situ* stretch, can be defined arbitrarily. Thus, this approach provides a basis for mechanical investigations that are specific for the considered type of artery.

The presented results demonstrate that the proposed model allows a detailed study of the mechanics of clamping procedures. The simulated three-dimensional deformations perfectly resemble the typical shape of compressed arteries, which, in contrast to previous studies, can be related with the stresses at any point of interest. Stress analyses revealed surprising effects: for example, the axial stresses in the media within the direct clamping area (see point *P* in Fig. 6) are four to five times higher than in the physiological state (Fig. 6). This effect is strongly influenced by the shape of the clamp jaws. Since the media is relatively vulnerable in regard to axial extension, this may be associated with medial damage and damage of the attached endothelial cells. This is not an obvious effect, is not described in the literature, and cannot easily be investigated with experimental methods. The relevance of stress analyses is underlined by the fact that even nondestructive loading, which exceeds the physiological limit, leads to biological responses that might be clinically adverse [46].

4.2 Limitations. In the present study cylindrical clamp jaws were chosen. This is not a typical geometry of real clamps. However, the goal of this study was to demonstrate the potential use of the proposed three-dimensional finite element model. We did not intend to evaluate particular clamp designs. This is left to subsequent studies.

Some of the data we used for the mechanical response of human arteries comes from an experimental study [39], that utilized a one-layer thin-walled arterial model. Actually, layer-specific mechanical data of human arteries are not available yet in the literature. Thus, for upcoming studies we plan to perform appropriate mechanical tests ourselves. Moreover, a realistic simulation of injuries requires appropriate constitutive models for the inelastic domain and tests beyond the (visco)elastic limit.

The presented finite element mesh is not capable of simulating a complete occlusion. This would require a mesh refinement at highly curved regions and the consideration of the contact between the opposite intimal layers.

Finally, in the downstream branch of the artery there is a decrease of the internal pressure p_i, which was not considered. A reduced internal pressure leads to lower wall stresses in clamped and non-clamped parts and consequently to less arterial injury. Thus, for investigations that are concerned with the risk of arterial injuries, only the upstream branch of the clamped artery is relevant.

4.3 Future Perspectives. The proposed concept may be extended to a ''virtual workbench,'' which allows one to investigate essential clinical questions. For example, the least damaging clamp design among existing clamps may be identified for a particular type of artery. Moreover, such a ''virtual workbench'' could guide optimal clamp designs. Regions of peak-stresses may be identified and avoided by means of constructive adaptations. Such investigations may consider injury thresholds of the involved tissues, in particular the intima [6]. In particular, the smallest width of a clamp, which does not lead to stresses beyond a certain injury threshold, may be determined. In addition, force-displacement curves of different clamp designs may be studied. This is of particular importance, since the reaction forces, sensed by the surgeon, allow a prompt response of the amount of compression. A good performance of a clamp, i.e. a pronounced increase of the reaction force at the state of total occlusion, might reduce wall injuries.

Acknowledgments

Financial support for this research was provided by the *Austrian Science Foundation* under *START-Award Y74-TEC*. This support is gratefully acknowledged.

References

[1] Dobrin, P. B., McGurrin, J. F., and McNulty, J. A., 1992, ''Chronic Histologic Changes After Vascular Clamping are Not Associated with Altered Vascular Mechanics,'' Ann. Vasc. Surg., **6**, pp. 153–159.
[2] Margovsky, A. I., Chambers, A. J., and Lord, R. S., 1999, ''The Effect of Increasing Clamping Forces on Endothelial and Arterial Wall Damage: An Experimental Study in the Sheep,'' Cardiovasc. Surg., **7**, pp. 457–463.
[3] Harvey, J. G., and Gough, M. H., 1981, ''A Comparison of the Traumatic Effects of Vascular Clamps,'' Br. J. Surg., **68**, pp. 267–272.
[4] Moore, W. M., Manship, L. L., and Bunt, T. J., 1985, ''Differential Endothelial Injury Caused by Vascular Clamps and Vessel Loops. I. Normal Vessels,'' Am. J. Surg., **51**, pp. 392–400.
[5] Manship, L. L., Moore, W. M., Bynoe, R., and Bunt, T. J., 1985, ''Differential Endothelial Enjury Caused by Vascular Clamps and Vessel Loops. II. Atherosclerotic Vessels,'' Am. J. Surg., **51**, pp. 401–406.
[6] Moore, Jr., W. M., Bunt, T. J., Hermann, G. D., and Fogarty, T. J., 1988, ''Assessment of Transmural Force During Application of Vascular Occlusive Devices,'' J. Vasc. Surg., **8**, pp. 422–427.
[7] Barone, G. W., Conerly, J. M., Farley, P. C., Flanagan, T. L., and Kron, I. L., 1989, ''Assessing Clamp-related Vascular Injuries by Measurement of Associated Vascular Dysfunction,'' Surgery, **105**, pp. 465–471.
[8] Gersak, B., Trobec, R., and Krisch, I., 1998, ''Loss of Endothelium Mediated Vascular Relaxation as a Response to Various Clamping Pressure. Part I. A Pharmacological Study,'' Panminerva Med., **40**, pp. 280–285.
[9] Gersak, B., Trobec, R., and Psenicnik, M., 1998, ''Loss of Endothelium Mediated Vascular Relaxation as a Response to Various Clamping Pressures. Part II. Direct Measurements of Clamping Pressures and Scanning Electron Microscope Study,'' Panminerva Med., **40**, pp. 286–293.
[10] Dujovny, M., Wakenhut, N., Kossovsky, N., Gomes, C. W., Laha, R. K., Leff, L., and Nelson, D., 1979, ''Minimum Vascular Occlusive Force,'' J. Neurosurg., **51**, pp. 662–668.
[11] Aukland, A., and Hurlow, R. A., 1981, ''Carotid Stenosis due to Clamp Injury,'' Br. J. Surg., **20**, pp. 282.
[12] Margovsky, A. I., Lord, R. S. A., Meek, A. C., and Bobryshev, Y. V., 1997, ''Artery Wall Damage and Platelet Uptake from so-called Atraumatic Arterial Clamps: An Experimental Study,'' Cardiovasc. Surg., **5**, pp. 42–47.

[13] Risberg, B., and Bylock, A., 1981, ''Vascular Trauma Induced by Clamping-correlation Between Surface Ultrastructure and Fibrinolytic Activity,'' Acta Chir. Scand., **147**, pp. 25–32.
[14] Margovsky, A. I., Lord, R. S. A., and Chambers, A. J., 1997, ''The Effect of Arterial Clamp Duration on Endothelial Injury: An Experimental Study,'' Aust. N. Z. J. Surg., **67**, pp. 448–451.
[15] Rhodin, J. A. G., 1980, ''Architecture of the Vessel Wall,'' *Handbook of Physiology, The Cardiovascular System*, edited by D. F. Bohr, A. D. Somlyo, and H. V. Sparks, 2, American Physiological Society, Bethesda, Maryland, pp. 1–31.
[16] Humphrey, J. D., 1995, ''Mechanics of the Arterial Wall: Review and Directions,'' Crit. Rev. Biomed. Eng., **23**, pp. 1–162.
[17] Holzapfel, G. A., Gasser, T. C., and Ogden, R. W., 2000, ''A New Constitutive Framework for Arterial Wall Mechanics and a Comparative Study of Material Models,'' J. Elast., **61**, pp. 1–48.
[18] Cox, R. H., 1978, ''Regional Variation of Series Elasticity in Canine Arterial Smooth Muscles,'' Am. J. Physiol., **234**, pp. H542–H551.
[19] Holzapfel, G. A., 2001, ''Biomechanics of Soft Tissue,'' *The Handbook of Materials Behavior Models. Volume III, Multiphysics Behaviors, Chapter 10, Composite Media, Biomaterials*, edited by J. Lemaitre, Academic Press, Boston, pp. 1049–1063.
[20] Holzapfel, G. A., and Gasser, T. C., 2001, ''A Viscoelastic Model for Fiber-reinforced Composites at Finite Strains: Continuum Basis, Computational Aspects and Applications,'' Comput. Methods Appl. Mech. Eng., **190**, pp. 4379–4403.
[21] Gasser, T. C., and Holzapfel, G. A., 2001, ''A Rate-independent Elastoplastic Constitutive Model for Biological Fiber-reinforced Composites at Finite Strains: Continuum Basis, Algorithmic Formulation and Finite Element Implementation,'' submitted.
[22] Patel, D. J., and Fry, D. L., 1969, ''The Elastic Symmetry of Arterial Segments in Dogs,'' Circ. Res., **24**, pp. 1–8.
[23] Carew, T. E., Vaishnav, R. N., and Patel, D. J., 1968, ''Compressibility of the Arterial Wall,'' Circ. Res., **23**, pp. 61–68.
[24] Holzapfel, G. A., 2000, *Nonlinear Solid Mechanics. A Continuum Approach for Engineering*, John Wiley & Sons, Chichester.
[25] Flory, P. J., 1961, ''Thermodynamic Relations for Highly Elastic Materials,'' Trans. Faraday Soc., **57**, pp. 829–838.
[26] Ogden, R. W., 1978, ''Nearly Isochoric Elastic Deformations: Application to Rubberlike Solids,'' J. Mech. Phys. Solids **26**, pp. 37–57.
[27] Holzapfel, G. A., Schulze-Bauer, C. A. J., and Stadler, M., 2000, ''Mechanics of Angioplasty: Wall, Balloon and Stent,'' *Mechanics in Biology*, edited by J. Casey and G. Bao, The American Society of Mechanical Engineers (ASME), New York, AMD-Vol. 242/BED-Vol. 46, pp. 141–156.
[28] Holzapfel, G. A., and Weizsäcker, H. W., 1998, ''Biomechanical Behavior of the Arterial Wall and its Numerical Characterization,'' Comput. Biol. Med., **28**, pp. 377–392.
[29] Roach, M. R., and Burton, A. C., 1957, ''The Reason for the Shape of the Distensibility Curve of Arteries,'' Canadian Journal of Biochemistry and Physiology, **35**, pp. 681–690.
[30] Spencer, A. J. M., 1984, ''Constitutive Theory for Strongly Anisotropic Solids,'' *Continuum Theory of the Mechanics of Fibre-Reinforced Composites*, edited by A. J. M. Spencer, Springer-Verlag, Wien, pp. 1–32, CISM Courses and Lectures No. 282, International Center for Mechanical Sciences.
[31] Vaishnav, R. N., and Vossoughi, J., 1983, ''Estimation of Residual Strains in Aortic Segments,'' *Biomedical Engineering II: Recent Developments*, edited by C. W. Hall, Pergamon Press, New York, pp. 330–333.
[32] Rodriguez, E. K., Hoger, A., and McCulloch, A. D., 1994, ''Stress-dependent Finite Growth in Soft Elastic Tissues,'' J. Biomech., **27**, pp. 455–467.
[33] Rachev, A., 1997, ''Theoretical Study of the Effect of Stress-dependent Remodeling on Arterial Geometry under Hypertensive Conditions,'' J. Biomech., **30**, pp. 819–827.
[34] Chuong, C. J., and Fung, Y. C., 1986, ''Residual Stress in Arteries,'' *Frontiers in Biomechanics*, edited by G. W. Schmid-Schönbein, S. L.-Y. Woo, and B. W. Zweifach, Springer-Verlag, New York, pp. 117–129.
[35] Johnson, B. E., and Hoger, A., 1998, ''The Use of Strain Energy to Quantify the Effect of Residual Stress on Mechanical Behavior,'' Math. Mech. Solids, **3**, pp. 447–470.
[36] Rachev, A., and Hayashi, K., 1999, ''Theoretical Study of the Effects of Vascular Smooth Muscle Contraction on Strain and Stress Distributions in Arteries,'' Ann. Biomed. Eng., **27**, pp. 459–468.
[37] Vossoughi, J., Hedjazi, Z., and Borris, F. S., 1993, ''Intimal Residual Stress and Strain in Large Arteries,'' *Bed-Vol. 24, 1993 Bioengineering Conference ASME*, pp. 434–437.
[38] Taylor, R. L., 2000, *FEAP—A Finite Element Analysis Program-Version 7.3*, University of California at Berkeley.
[39] Carmines, D. V., McElhaney, J. H., and Stack, R., 1991, ''A Piece-wise Nonlinear Elastic Stress Expression of Human and Pig Coronary Arteries Tested *in vitro*,'' J. Biomech., **24**, pp. 899–906.
[40] Yu, Q., Zhou, J., and Fung, Y. C., 1993, ''Neutral Axis Location in Bending and Young's Modulus of Different Layers of Arterial Wall,'' Am. J. Physiol., **265**, pp. H52–H60.
[41] Simo, J. C., Taylor, R. L., and Pister, K. S., 1985, ''Variational and Projection Methods for the Volume Constraint in Finite Deformation Elasto-plasticity,'' Comput. Methods Appl. Mech. Eng., **51**, pp. 177–208.
[42] Nagtegaal, J. C., Parks, D. M., and Rice, J. R., 1974, ''On Numerically Accurate Finite Element Solutions in the Fully Plastic Range,'' Comput. Methods Appl. Mech. Eng., **4**, pp. 153–177.
[43] Nichols, W. W. and O'Rourke, M. F., 1998, *McDonald's Blood Flow in Arteries*, chap. 4, Arnold, London, 4th ed., pp. 73–97.
[44] Xie, J., Zhou, J., and Fung, Y. C., 1995, ''Bending of Blood Vessel Wall: Stress-strain Laws of the Intima-Media and Adventitia Layers,'' J. Biomech. Eng., **117**, pp. 136–145.
[45] Slayback, J. B., Bowen, W. W., and Hinshaw, D. B., 1976, ''Intimal Injury from Arterial Clamps,'' Am. J. Surg., **132**, pp. 183–188.
[46] Jackiewicz, T. A., McGeachie, J. K., and Tennant, M., 1996, ''Structural Recovery of Small Arteries Following Clamp Injury: A Light and Electron Microscopic Investigation in the Rat,'' Microsurgery, **17**, pp. 674–680.